Applied Catalysis A: General 427–428 (2012) 43–48

Contents lists available at SciVerse ScienceDirect

Applied Catalysis A: General

journal homepage: www.elsevier.com/locate/apcata

Catalytic reduction of NO by NH_3 over Fe–Cu–O_X/CNTs-TiO_2 composites at low temperature

Zhaoxia Ma, Hangsheng Yang*, Qian Li, Junwei Zheng, Xiaobin Zhang

State Key Laboratory of Silicon Materials, Department of Materials Science and Engineering, Zhejiang University, Zheda Road 38, Hangzhou 310027, China

ARTICLE INFO

Article history:
Received 13 January 2012
Received in revised form 17 March 2012
Accepted 19 March 2012
Available online 28 March 2012

Keywords:
Selective catalytic reduction
Carbon nanotubes
Iron–copper oxides
NO oxidation

ABSTRACT

Activity of iron–copper oxides supported on TiO_2 and carbon nanotubes (CNTs) for low-temperature selective catalytic reduction of NO by NH_3 in the presence of oxygen was investigated. The addition of FeO_X and CNTs synergistically promoted the NO conversion through the adsorption of NO and NH_3 and the catalytic oxidation of NO to NO_2. NO_2 adsorbed on the surface of the catalysts was found to be essential for NO reduction at low temperature, and approximately 90% NO conversion could be achieved at reaction temperature as low as 150 °C. Moreover, it was found that the deactivation caused by H_2O could be recovered after H_2O was switched off, while the deactivation caused by SO_2 was dependent on the reaction temperature.

1. Introduction

Nitrogen oxides (NO_X), which induce the formation of acid rain and ground-level ozone and cause respiratory problems, are therefore harmful for the ecosystem and humanity. Selective catalytic reduction (SCR) of NO_X by NH_3 in the presence of oxygen is one of the most effective methods to decrease the NO_X levels in gaseous emissions [1]. In recent decades, a variety of SCR catalysts have been developed for possible application, which can be divided into three groups, namely, noble metals, ion-exchanged zeolites, and metal oxides. Among them, V_2O_5-WO_3/TiO_2 has been widely accepted as an industrial catalyst despite the fact that vanadium protoxide is toxic and V_2O_5-WO_3/TiO_2 is only active within a narrow and high temperature window (300–400 °C) [2–5]. So it is necessary to develop novel catalysts to reduce the vanadium loadings or replace the vanadium with other metal elements. For this reason, many researchers continue to modify current catalysts. Moreno-Tost et al. [6] investigated cobalt–iridium supported on zirconium-doped mesoporous silica as catalysts for NH_3-SCR and found out Co–Ir supported catalysts showed higher NO conversion than Co supported catalyst. Wu et al. [7] reported a MnO_X–CeO_2 catalyst which has a high NO_X conversion within a low temperature range (80–220 °C). Lu et al. [8] reported that CeO_2 supported on ACF obtained 70% NO conversion at 150 °C.

Cu and Fe are two of the typically studied transition metals in SCR catalysts. Catalytic behaviors of Cu and Fe zeolites in the NH_3-SCR of NO [9,10] as well as in the HC-SCR of NO_X have been studied systematically [11,12]. Also, copper oxides and iron oxides, supported on Al_2O_3 [13], TiO_2 [14], SiO_2 [15], ZrO_2 [16], and carbonaceous material [17,18], are found to be active in medium temperature SCR of NO. However, exhaust gases usually contain a large amount of fly ash and SO_2, which severely deactivate the catalysts. Thus, further lowering the de-NO_X temperature is necessary so that SCR systems can be installed downstream of the desulfurizer and the electrostatic precipitator.

Recently, it was reported that carbon nanotubes (CNTs) are good adsorbents of NO_2, O_2, VOCs and NH_3 [19]. We also found that the addition of CNTs was beneficial for the SCR of de-NO_X and De-VOCs over a variety of metal oxide catalysts [20–22]. Based on our foregoing research, we prepared CNTs and TiO_2-supported iron and copper oxides by sol–gel method and studied their performance for NO reduction at low temperatures in the present study.

2. Experimental

2.1. Catalyst preparation

The catalysts were prepared by a sol–gel method. The purified CNTs [23] were first sonicated in ethanol for 30 min for good dispersion. Tetrabutyl titanate was then added, and the solution was sonicated for another 30 min. Copper nitrate [$Cu(NO_3)_2{\cdot}3H_2O$], ferric nitrate [$Fe(NO_3)_3{\cdot}9H_2O$], and acetic acid were dissolved in distilled water and ethanol and added into the above solution. The resulting solution was sonicated until sols were formed. The sols were aged at ambient conditions to obtain good gels, which were air-dried at 100 °C overnight and then calcined at 500 °C for 4 h in

* Corresponding author. Tel.: +86 571 87951404; fax: +86 571 87951404.
E-mail address: hsyang@zju.edu.cn (H. Yang).

0926-860X/$ – see front matter © 2012 Elsevier B.V. All rights reserved.
doi:10.1016/j.apcata.2012.03.028

Table 1
Summary of the catalysts prepared via the sol–gel method.

Catalysts	Cu:Fe (wt%:wt%)[a]	CNTs (wt%)[b]	Surface atomic ratio (%)[c]		S_{BET} (m^2/g)	Catalyst label
			Cu/Ti	Fe/Ti		
CuO_X/CNTs-TiO_2	–	5	0.39	–	97.2	$Cu_{10}Ti_{85}C_5$
	3:1	5	0.30	0.15	80.8	$Cu_3Fe_1Ti_{85}C_5$
	2:1	5	0.25	0.23	76.9	$Cu_2Fe_1Ti_{85}C_5$
Fe–Cu–O_X/CNTs-TiO_2	1:1	5	0.24	0.25	76.8	$Cu_1Fe_1Ti_{85}C_5$
	1:2	5	0.22	0.27	85.1	$Cu_1Fe_2Ti_{85}C_5$
	1:3	5	0.26	0.31	50.8	$Cu_1Fe_3Ti_{85}C_5$
FeO_X/CNTs-TiO_2	0	5	–	0.36	56.0	$Fe_{10}Ti_{85}C_5$
Fe–Cu–O_X/TiO_2	1:1	0	0.31	0.26	73.0	$Cu_1Fe_1Ti_{90}$

[a] Mass ratio of the Cu and Fe atoms when added to the system.
[b] Mass ratio of CNTs when added to the system.
[c] Surface atomic ratio as determined by XPS.

a N_2 atmosphere to acquire Fe–Cu–O_X/CNTs-TiO_2. Seven samples were analyzed to investigate the effect of Cu:Fe ratio and CNTs on low-temperature SCR of NO by NH_3. The samples had the same 10% Cu + Fe loading with different Cu:Fe ratios and a mass fraction of 5% CNTs as shown in Table 1.

2.2. Characterization

X-ray diffraction (XRD) patterns were recorded on a Philips XD-98 X-ray diffractometer with Kα radiation (λ = 0.15406 nm). A Hitachi S-4800 scanning electron microscope (SEM) was used to characterize the morphologies of the samples. Brunauer–Emmett–Teller (BET) surface areas were measured using an ASAP2000 physical adsorber. X-ray photoelectron spectroscopy (XPS) data were obtained using a Thermo ESCALAB 250. The X-ray source was an Al Kα radiation. All binding energies were referenced to a 284.8 eV C1s.

H_2-temperature-programmed reduction (H_2-TPR) experiments were performed using 50 mg of each catalyst. The samples were pretreated under a N_2 gas flow from 40 °C to 400 °C at a temperature increment of 10 °C/min. TPR experiments were performed at a heating rate of 10 °C/min under a mixed flow of 5% H_2 in argon at a flow rate of 40 ml/min. NH_3-temperature-programmed desorption (NH_3-TPD) experiments were performed using 50 mg of each catalyst to determine their NH_3 adsorption ability. The sample was pretreated in a N_2 stream (30 ml/min) at 400 °C for 1 h, then cooled to 100 °C. The pretreated sample was exposed to a mixed flow of 4% NH_3 in argon at a flow rate of 20 ml/min for 3 h at ambient temperature, and then heated from 100 °C to 850 °C at a heating rate of 10 °C/min. The H_2-TPR and NH_3-TPD data were recorded using an on-line gas chromatograph equipped with a thermal conductivity detector.

NO oxidation experiments were performed on the catalysts using an NO-NO_2-NO_X analyzer (Testo AG testo 350) to record the NO and NO_2 signals. The catalysts were heated from 100 °C to 410 °C, and 550 ppm of NO was fed in the presence of oxygen (5%, v/v) and a N_2 balance at a total flow rate of 500 ml/min and a gas hourly space velocity (GHSV) of 36,000 h^{-1}.

NO_X-temperature-programmed desorption (NO_X-TPD) experiments were performed on the catalysts using Testo AG testo 350 to record the NO and NO_2 signals. The samples were exposed to a 550 ppm NO flow and 5 vol% O_2 for 2 h at 400 °C and cooled to 100 °C in the same gas stream, followed by a N_2 purge during sample cooling to 80 °C. Once the NO signal returned to the baseline level, the temperature was ramped from 80 °C to 420 °C in N_2 at a rate of 10 °C/min.

FT-IR experiments were performed on $Cu_3Fe_1Ti_{85}C_5$ catalyst recorded with a Nicolet 5700 Fourier Transform spectrometer (0.09 cm^{-1} resolution). $Cu_3Fe_1Ti_{85}C_5$ catalyst was pretreated under an Ar gas flow (200 ml/min) at 100 °C overnight, then the catalyst was cooled to room temperature (RT) and exposed to a mixed flow of 1000 ppm NO and 5% O_2 at RT for 12 h, followed by an Ar purge at RT, then the samples were exposed to a mixed flow of 2% NH_3 in Ar at a flow rate of 30 ml/min for 2 h at RT, 100 °C, 200 °C, 250 °C respectively, following an Ar purge when the samples were cooled down. The powder samples at every stage were compressed in KBr-supporting disks to obtain the IR spectra.

2.3. Catalytic activity measurement

SCR activity measurements were conducted in a fixed-bed flow reactor. All samples were ground and mixed with 25 wt% organoclay and pasted on 3 cm × 10 cm aluminum plates. Ten catalytic plates were placed in a reactive tank with a 5 mm interval [21,24]. The reaction conditions were as follows: 550 ppm NO, 550 ppm NH_3, 5 vol% O_2 balanced by N_2 at a total flow rate of 500 ml/min. The inlet and outlet concentrations of NO, NO_2, and O_2 were monitored using an NO-NO_2-NO_X analyzer (Testo AG testo 350). The SCR activity tests were performed at reaction temperatures between 100 °C and 300 °C at a GHSV of 36,000 h^{-1}.

3. Results

3.1. SCR activity

Catalytic performances of a series of catalysts are shown in Fig. 1. $Cu_1Fe_1Ti_{90}$ was almost inactive up to 175 °C, then, NO conversion monotonically increased with temperature, reaching 32% and 94.37% at 200 and 300 °C, respectively. The NO conversion

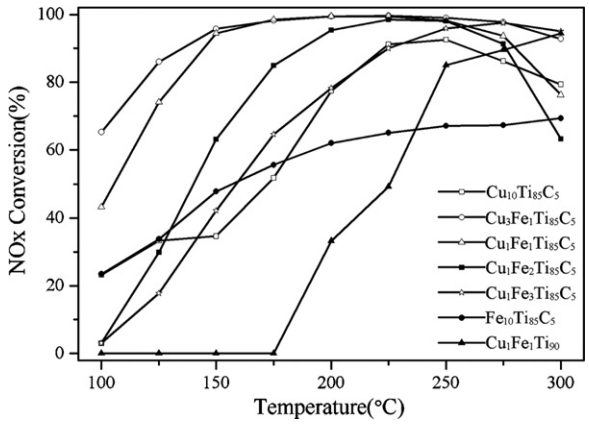

Fig. 1. NO_X conversion over the Fe–Cu–O_X/CNTs-TiO_2 catalysts, at 550 ppm NO, 550 ppm NH_3, 5% O_2, and 36,000 h^{-1} GHSV.

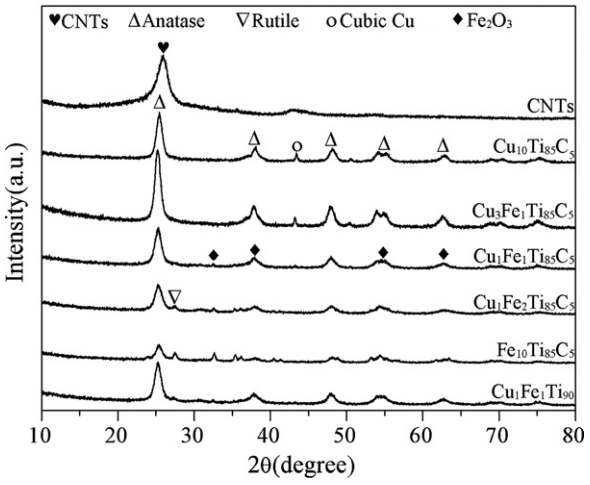

Fig. 2. XRD patterns of the CNTs and the Fe–Cu–O_X/CNTs-TiO_2 catalysts.

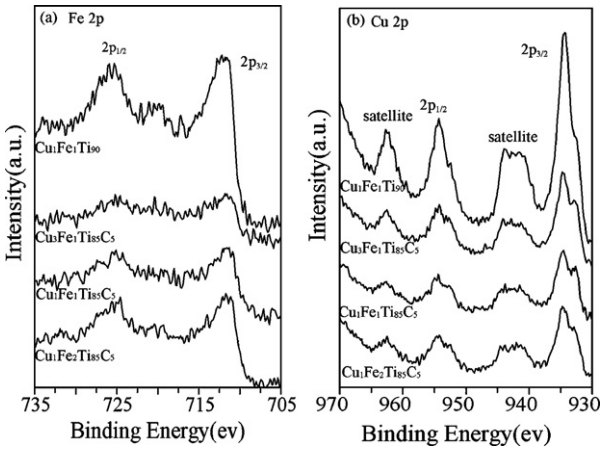

Fig. 4. XPS results of (a) Fe 2p and (b) Cu 2p in $Cu_1Fe_1Ti_{90}$, $Cu_3Fe_1Ti_{85}C_5$, $Cu_1Fe_1Ti_{85}C_5$, and $Cu_1Fe_2Ti_{85}C_5$.

markedly increased with the addition of the CNTs. Approximately 42% of NO was converted over $Cu_1Fe_1Ti_{85}C_5$ at the low temperature of 100 °C, and 90% conversion was achieved at temperatures between 150 and 275 °C. These results are in good agreement with our previous reports [21,24,25]. Note that, the NO conversion over Fe–Cu–O_X/CNTs-TiO_2 increased with increasing Cu:Fe atomic ratio (from 1:3 to 3:1); in particular, 99% NO conversion was achieved over $Cu_3Fe_1Ti_{85}C_5$ at 175–250 °C. Fig. 1 also shows that the activity of $Cu_{10}Ti_{85}C_5$ is higher than that of $Fe_{10}Ti_{85}C_5$, especially at temperatures above 175 °C, a NO conversion of 23.4–92.57% was obtained over $Cu_{10}Ti_{85}C_5$ at 100 °C to 250 °C, compared to the 23.4–69.32% conversion over $Fe_{10}Ti_{85}C_5$. And the NO conversion over $Cu_1Fe_1Ti_{85}C_5$ at temperatures below 150 °C was higher than the sum of those over $Cu_{10}Ti_{85}C_5$ and $Fe_{10}Ti_{85}C_5$, suggesting a possible synergistic effect between FeO_X and CuO_X with the assistance of CNTs.

3.2. XRD, SEM and BET studies

The X-ray diffractograms of CNTs and Fe–Cu–O_X/CNTs-TiO_2 composites are shown in Fig. 2. The primary crystal phase of all TiO_2-supported catalysts was anatase, and the (0 0 2) reflection of the CNTs at 26.4° was overlapped by the anatase (1 0 1) reflection at 25.3°. Moreover, the full width at half maximum (FWHM) of the anatase (1 0 1) peaks for all samples were similar, suggesting similar TiO_2 grain sizes in all samples. No peaks attributed to copper oxides were detected, suggesting that the copper oxides existed as a monolayer [26] or highly dispersed on the surface of TiO_2 and CNTs. A weak peak corresponding to cubic Cu crystallites was observed (2θ = 43.32) over $Cu_{10}Ti_{85}C_5$ and $Cu_3Fe_1Ti_{85}C_5$, possibly due to partial reduction of CuO_X by carbon in the thermal treatment during catalyst preparation. The FeO_X phase was mainly Fe_2O_3 crystallite detected by XRD. By the way, weak peaks attributed to rutile were observed from $Cu_1Fe_1Ti_{90}$, $Fe_{10}Ti_{85}C_5$, and $Cu_1Fe_2Ti_{85}C_5$, the additions of FeO_X may promote the formation of the rutile phase [27]. Since TiO_2 is almost inactive in the 100–300 °C reaction temperature range [28], the influence of the small amount of rutile on the catalytic activity was neglected.

Typical SEM images of the as-prepared $Cu_1Fe_1Ti_{90}$ and Fe–Cu–O_X/CNTs-TiO_2 catalysts are shown in Fig. 3. The agglomeration of the $Cu_1Fe_1Ti_{90}$ catalyst particles was observed. In contrast, a good dispersion of the active components on the CNT surfaces was achieved as shown in Figs. 3b–d. Moreover, the correlation between catalytic performance and BET surface area was not established, as shown in Table 1, $Cu_{10}Ti_{85}C_5$ catalyst had the largest BET surface area, but the catalytic performance was not the best.

3.3. XPS analysis

Fig. 4 shows the XPS spectra of $Cu_1Fe_1Ti_{90}$, $Cu_3Fe_1Ti_{85}C_5$, $Cu_1Fe_1Ti_{85}C_5$, and $Cu_1Fe_2Ti_{85}C_5$. The binding energies of Fe $2p_{3/2}$ (711–711.8 eV) and Fe $2p_{1/2}$ (724.6–725.1 eV) [29] corresponded well with the Fe^{3+} species, and were in good agreement with XRD results. Broad peaks of Cu corresponded to the different copper oxides, namely, Cu_2O (932.6 and 952.5 eV) and CuO (934.7 and 954.5 eV) [30,31]. The intensity of the Cu^+ peak was much lower than that of Cu^{2+}, indicating that Cu mainly existed as CuO. The addition of CNTs reduced the peak intensities of Cu and Fe, indicating that CNTs promoted the dispersion of the active components, since the BET surface area increased accordingly as was summarized in Table 1. When the molar ratio of Fe:Cu was increased from 1:3 to 3:1, the real surface atomic ratio is different from the additive amount and the Fe/Ti ratio was increased from 0.15 to 0.31,

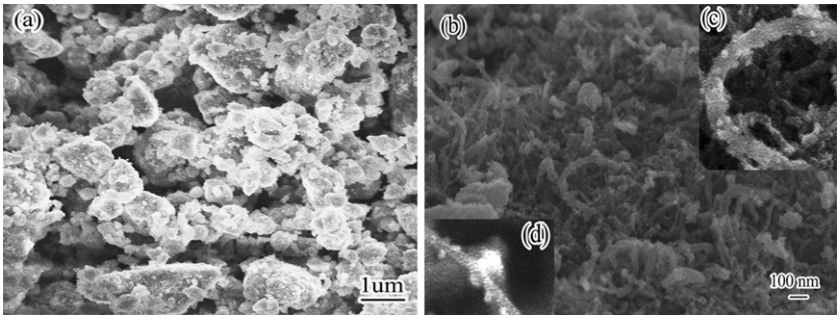

Fig. 3. SEM images of (a) $Cu_1Fe_1Ti_{90}$; (b–d) Fe–Cu–O_X/CNTs-TiO_2.

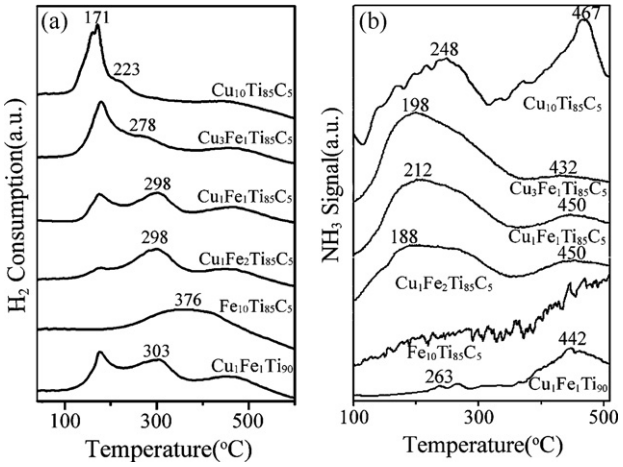

Fig. 5. H_2-TPR (a) and NH_3-TPD (b) profiles of the Fe–Cu–O_X/CNTs-TiO_2 catalysts.

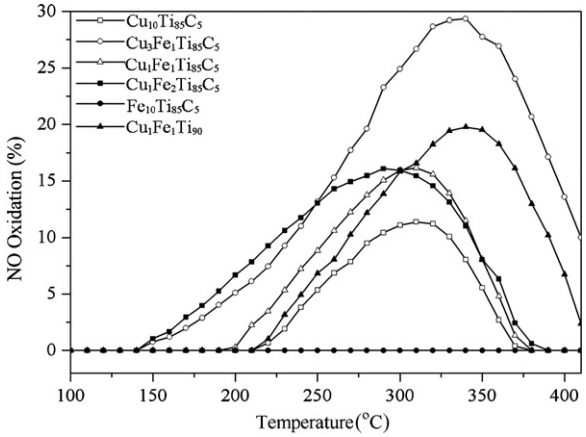

Fig. 6. Oxidation of NO to NO_2 by O_2 over the Fe–Cu–O_X/CNTs-TiO_2 catalysts. Reaction conditions: [NO] = 550 ppm, [O_2] = 5%, balance N_2, and GHSV = 36,000 h^{-1}.

also, the surface Cu/Ti ratio decreased from 0.30 to 0.22 when the Fe:Cu was increased from 1:3 to 2:1. It seems the copper species has better dispersibility, therefore, no CuO_X related XRD peaks was detected as shown in Fig. 2.

3.4. H_2-TPR and NH_3-TPD

H_2-TPR profiles of Fe–Cu–O_X/CNTs-TiO_2 and $Cu_1Fe_1Ti_{90}$ are shown in Fig. 5a. For $Cu_{10}Ti_{85}C_5$, two convoluted reduction peaks appeared at 171 °C and 223 °C, which are ascribed to the sequential reduction of: (1) highly dispersed CuO species in close interaction with the TiO_2 and CNTs support (171 °C), (2) reduction of small and dispersed oxide clusters not forming crystallites yet (223 °C) [32]. The TPR curve of $Fe_{10}Ti_{85}C_5$ shows two overlap peaks at 220 °C to 500 °C, conforming the stepwise reduction of Fe_2O_3 by H_2 as $Fe_2O_3 \rightarrow Fe_3O_4 \rightarrow Fe$ [33]. The catalysts containing both Cu and Fe showed peaks at about 171 °C, 278–303 °C, and 380–470 °C, respectively. The appearance of a new peak at 278–303 °C suggests the possible interaction between FeO_X and CuO_X.

The NH_3-TPD technique was employed to determine the acidic sites in the catalysts. As shown in Fig. 5b, the peaks observed below 200 °C and between 200 °C and 340 °C could be attributed to the NH_3 desorbed by weak and medium acid sites on $Cu_{10}Ti_{85}C_5$, respectively; the peaks above 340 °C could be attributed to the chemisorbed NH_3 molecules adsorbed by the strong acid sites [34]. Fig. 5b also indicates that NH_3 was still absorbed on all of the catalysts at temperature higher than reaction temperature.

3.5. NO to NO_2 oxidation and NO_X TPD

According to literature [10,25,35–37], the existence of NO_2 can accelerate the SCR reaction through a fast reaction of $2NH_3 + NO + NO_2 \rightarrow 2N_2 + 3H_2O$. Therefore, the NO oxidation as a function of reaction temperature was studied and is shown in Fig. 6. No signal of gaseous NO_2 over $Fe_{10}Ti_{85}C_5$ was detected within the entire reaction temperature range. The reaction over the $Cu_{10}Ti_{85}C_5$ catalyst at low temperatures was kinetically limited [10]. NO conversion was kept at 0% below 220 °C, then NO oxidation increased with temperature, and reached the maximum of 11.37% at 310 °C. The NO oxidation efficiency decreased with further increasing the temperature due to the thermodynamic limits [10]. These results suggest that CuO_X has better catalytic activity to promote NO oxidation ability than FeO_X. From Fig. 6, the $Cu_{10}Ti_{85}C_5$, $Fe_{10}Ti_{85}C_5$, $Cu_1Fe_1Ti_{90}$ and $Cu_3Fe_1Ti_{85}C_5$ catalysts achieved their highest NO oxidation of 11.37% (310 °C), 0%, 19.78% (340 °C) and 29.36% (340 °C), respectively. These results demonstrate that the addition of FeO_X which cannot oxidize NO strengthened the oxidation activity of the catalysts, especially with the assistance of CNTs. This is in good agreement with our previous results that the addition of CNTs promoted the oxidation of NO to NO_2 over V_2O_5/TiO_2 catalyst [25].

Adsorption of NO_X species on the catalyst surface was reported to play an important role in NO reduction [37]. Fig. 7 shows the NO_X desorption profiles of this series of catalysts. In the presence of oxygen, NO can form nitrite species or strongly bind nitrate species, which decompose to NO and NO_2 at high temperatures [37]. The ranking of the NO_2-TPD peak was: $Fe_{10}Ti_{85}C_5$ (250 °C) < $Cu_{10}Ti_{85}C_5$ (310 °C) = $Cu_3Fe_1Ti_{85}C_5$ (310 °C) < $Cu_1Fe_1Ti_{85}C_5$ (330 °C) < $Cu_1Fe_2Ti_{85}C_5$ (350 °C) = $Cu_1Fe_1Ti_{90}$ (350 °C), with a detected NO_2 concentration of 14.9, 64.9, 642.7, 154.4, 370.8, and 150.2 ppm, respectively. Also NO_2 is desorbed 50 °C before NO except $Fe_{10}Ti_{85}C_5$. The NO_2 ($NO + NO_2$) concentration desorbed from catalysts of $Fe_{10}Ti_{85}C_5$, $Cu_{10}Ti_{85}C_5$, $Cu_1Fe_1Ti_{90}$ and $Cu_3Fe_1Ti_{85}C_5$; were 0.15 (0.57), 1.77 (2.85), 2.50 (3.02) and 11.53 (27.95) ppm/mg, respectively. This indicates that the addition of FeO_X and CNTs [38] promoted the NO_2 adsorption on the catalyst surface, which could be the possible reason for the synergistic effect between the CuO_X and FeO_X.

3.6. Effect of H_2O and SO_2 on SCR activity

H_2O and SO_2 are the main components of exhaust gas and are detrimental to NO_X removal. As shown in Fig. 8, when 10% H_2O was added in the feed gas at 225 °C, the NO_X conversion decreased from 99% to 65% quickly over the $Cu_3Fe_1Ti_{85}C_5$, and then recovered gradually and remained at approximately 85%. When H_2O flow was stopped, the activity completely recovered and kept unchanged during the succeeding 6 h of the test. It seems the decrease in the NO_X conversion was caused by the competitive adsorption of H_2O and the reactant NH_3 [39].

When SO_2 was introduced at 225 °C, as shown in the inset of Fig. 8, the NO_X removal efficiency decreased from 99% to 84% immediately and then further decreased to 70%. The efficiency kept at a low level (70%) even after the SO_2 introduction was stopped, suggesting a deactivation of catalyst. At 250 °C, NO_X conversion also decreased to 81–84%. However, NO_X conversion recovered to 88.34% when the SO_2 supply was switched off, indicating a partial recovery of catalyst deactivation. According to literature [40,41], the deposition of sulfates and bisulfates was a possible reason for deactivation. However, the decomposition temperature of these species could decrease in the presence of activated carbon (AC) [42]. Similarly, in the present study, the addition of CNTs seems to

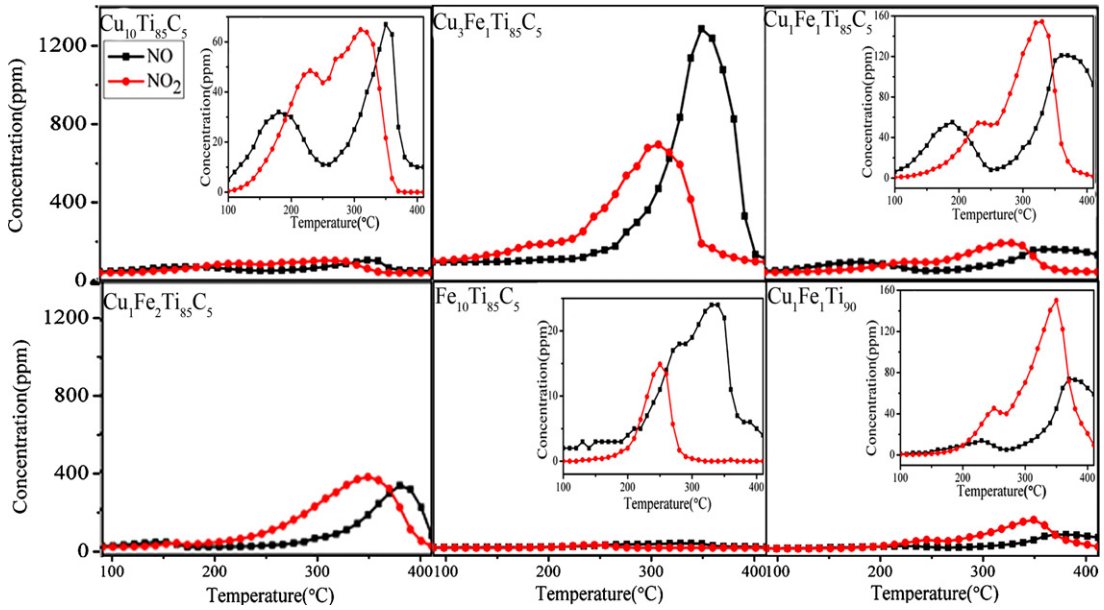

Fig. 7. NO_X-TPD profiles of the Fe–Cu–O_X/CNTs-TiO_2 catalysts dosed with NO/O_2 at 400 °C and then cooled to 100 °C in NO/O_2 prior to temperature ramping.

reduce the decomposition temperature of sulfates and bisulfates, as a result, SO_2 deactivation was partly suppressed at 250 °C.

4. Discussion

The correlation among the catalytic performance, NO oxidation, and NO_X desorption of the catalysts could be established according to Figs. 1, 6 and 7. The NO_2 concentrations detected in the gas phase over this series of catalysts were relatively low (Fig. 6), which could be due to the dependence of the NO oxidation rate on the NO_2 adsorption [43]. The NO_2 TPD results in Fig. 7 supported this assumption, since NO_2 was strongly adsorbed on the catalysts, thus suppressed further oxidation of NO. The NO_2 desorption peak of all the catalysts occurred between 310 and 350 °C, which is higher than the temperatures needed for NO reduction as shown in Fig. 1. Moreover, the NO desorption peak is 50 °C higher than that of NO_2 except $Fe_{10}Ti_{85}C_5$. These results indicate that NO_X species were adsorbed on the surface during reduction in this study. Moreover, the addition of CNTs were found to promote the active components dispersion, the oxidation of NO to NO_2, thus beneficial for NO_X reduction.

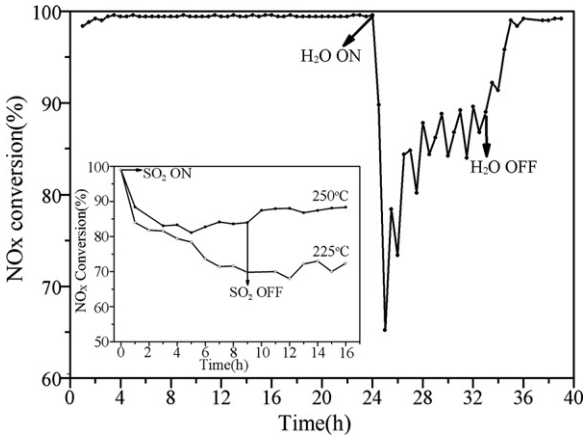

Fig. 8. Effect of H_2O on NO_X conversion over $Cu_3Fe_1Ti_{85}C_5$, reaction conditions: [NO] = 550 ppm, [NH_3] = 550 ppm, [O_2] = 5%, [H_2O] = 10%, balance N_2, and GHSV = 36,000 h^{-1} at 225 °C. The inset is effect of SO_2 on NO_X conversion over $Cu_3Fe_1Ti_{85}C_5$, reaction conditions: [NO] = 550 ppm, [NH_3] = 550 ppm, [O_2] = 5%, [SO_2] = 200 ppm,balance N_2, and GHSV = 36,000 h^{-1}.

The Langmuir–Hinshelwood (L–H) [44–46] and Eley–Rideal (E–R) [16,47,48] mechanisms are two of the most accepted mechanisms proposed in normal SCR systems. In the present study, for the $Fe_{10}Ti_{85}C_5$ catalyst, the amount of adsorbed NO_X is negligible (Fig. 7). Therefore, the reaction between adsorbed NH_3 and gas phase or weakly adsorbed NO is the primary route which followed the E–R mechanism. For other catalysts, however, the decrease of NO reduction efficiency at temperatures above 250 °C (Fig. 1) is accompanied with the desorption of NO_2, though the NO_2 concentration in gas phase is also detected and NO is still adsorbed on the catalyst surface at 300 °C (Fig. 7). This suggests that the adsorbed NO_2 plays an important role for SCR of NO at temperature below 250 °C. At high reaction temperature above 250 °C, the desorbed NO_2 in gas phase and the adsorbed NO are also considered to contribute to the NO reduction. Based on the above discussion, in the present study, NO_X reduction are possible to follow both E–R and L–H mechanisms. At low reaction temperatures, however, it seems NO_X reduction mainly followed the L–H mechanism through the reaction between adsorbed NO_2 and adsorbed NH_3.

In order to further confirm this assumption, catalyst $Cu_3Fe_1Ti_{85}C_5$ at different reaction stages were studied by FT-IR. As shown in Fig. 9a, no FT-IR peaks attributed to NO_2^- and NO_3^- were observed from Ar purged catalyst (curve a). When the catalyst was exposed to NO/O_2 (curve b), a strong peak at 1380 cm^{-1}, together with four weak peaks at 1619 cm^{-1}, 1564 cm^{-1}, 1520 cm^{-1}, and 1340 cm^{-1} were observed. The peak at 1380 cm^{-1} is attributed to the NO_2^- (monodentate nitrito), and the peaks at 1340 cm^{-1} and 1520 cm^{-1} are due to NO_2^- (chelated nitro); the peaks at 1564 cm^{-1} and 1619 cm^{-1} are attributed to bidentate NO_3^- [49,50]. These IR peaks indicated that both NO_2 and NO are adsorbed on the catalyst surface. After the catalyst was exposed to NH_3 for 2 h at room temperature (curve c), the IR peaks at 1564 cm^{-1} and 1619 cm^{-1} weakened evidently, suggesting the reaction between adsorbed NO_2 (NO_3^-) and adsorbed NH_3, but the peaks at 1520 cm^{-1}, 1380 cm^{-1}, and 1340 cm^{-1} were still detected, suggesting that the adsorbed NO (NO_2^-) cannot react with NH_3 at room temperature. After the catalyst was exposed to NH_3 at 100 °C (curve d), IR peaks attributed to NO_3^- disappeared, indicating the

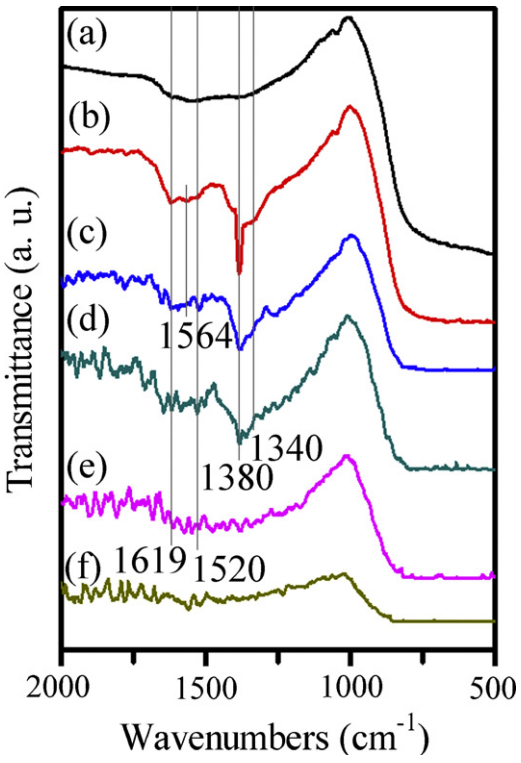

Fig. 9. FT-IR spectra of (a) $Cu_3Fe_1Ti_{85}C_5$ after Ar purging; (b) after the adsorption of NO/O_2 mixture at room temperature; (c–f) the NO_X adsorbed catalysts reacted with NH_3 at, room temperature, 100 °C, 200 °C, and 250 °C, respectively.

consumption of adsorbed NO_2, which suggests that the reaction between adsorbed NO_2 and adsorbed NH_3 occurred at reaction temperature below 100 °C. After the catalyst was reacted with NH_3 at 200 °C and/or 250 °C (curves e and f), the adsorbed NO_2^- species (peaks at 1380 and 1340 cm^{-1}) were also totally consumed. These results shown in Fig. 9 provided further evidence that the NO_X reduction in this study mainly followed the L–H mechanism through the reaction between adsorbed NO_X (especially NO_2) and adsorbed NH_3 at temperature below 200 °C, since the NO_X were confirmed to be still adsorbed on the catalyst surface as shown in Fig. 7.

5. Conclusions

In summary, iron–copper oxides supported on TiO_2 and CNTs showed high de-NO_X activity up to 99% at low reaction temperatures between 175 and 250 °C in the presence of oxygen. A synergistic interaction between CuO_X and FeO_X was observed with the addition of CNTs. The adsorbed NO_2 on the catalyst surfaces was essential for NO_X reduction at low temperature. Also the catalysts showed a relative high resistance to H_2O and SO_2 deactivation.

Acknowledgments

This work was supported by the Environmentally Sustainable Management of Medical Wastes in China (Contract No. C/V/S/10/251), the National Natural Foundation of Zhejiang Province, China (Grant No. Z4080070), the Foundation of Science and Technology Bureau of Zhejiang Province, China (Grant Nos. 2008C21057 and 2009C34003), and the Fundamental Research Funds for the Central Universities (Program No. 2010QNA4005).

References

[1] Z.M. Liu, S.I. Woo, Catal. Rev. Sci. Eng. 48 (2006) 43–89.
[2] O. Kröcher, M. Elsener, Ind. Eng. Chem. Res. 47 (2008) 8588–8593.
[3] G. Busca, L. Lietti, G. Ramis, F. Berti, Appl. Catal. B 18 (1998) 1–36.
[4] S. Roy, A. Baiker, Chem. Rev. 109 (2009) 4054–4091.
[5] P. Balle, B. Geiger, S. Kureti, Appl. Catal. B 85 (2009) 109–119.
[6] R. Moreno-Tost, E.R. Castellon, A. Jimenez-Lopez, J. Mol. Catal. A 248 (2006) 126–134.
[7] Z. Wu, B. Jiang, Y. Liu, Appl. Catal. B 79 (2008) 347–355.
[8] P. Lu, C.T. Li, G.M. Zeng, L.J. He, D.L. Peng, H.F. Cui, S.H. Li, Y.B. Zhai, Appl. Catal. B 96 (2010) 157–161.
[9] A. Sultana, T. Nanba, M. Haneda, M. Sasaki, H. Hamada, Appl. Catal. B 101 (2010) 61–67.
[10] M. Devadas, O. Kröcher, M. Elsener, A. Wokaun, N. Söger, M. Pfeifer, Y. Demel, L. Mussma, Appl. Catal. B 67 (2006) 187–196.
[11] A. Sultana, T. Nanba, M. Haneda, H. Hamada, Catal. Commun. 10 (2009) 1859–1863.
[12] B. Wichterlova, Top. Catal. 28 (2004) 131–140.
[13] L. Chmielarz, P. Kustrowski, M. Zbroja, B. Gil-Knap, J. Datka, R. Dziembaj, Appl. Catal. B 53 (2004) 47–61.
[14] D.A. Peña, B.S. Uphade, P.G. Smirniotis, J. Catal. 221 (2004) 421–431.
[15] J. Huang, Z. Tong, Y. Huang, J. Zhang, Appl. Catal. B 78 (2008) 309–314.
[16] N. Apostolescu, B. Geiger, K. Hizbullah, M.T. Jan, S. Kureti, D. Reichert, F. Schott, W. Weisweiler, Appl. Catal. B 62 (2006) 104–114.
[17] H.S. Teng, L.Y. Hsu, Y.C. Lai, Environ. Sci. Technol. 35 (2001) 2369–2374.
[18] M.J. Illán-Gómez, E. Raymundo-Piñero, A. García-García, A. Linares-Solano, C.S.M. de Lecea, Appl. Catal. B 20 (1999) 267–275.
[19] S. Santucci, S. Picozzi, F. Di Gregorio, L. Lozzi, J. Chem. Phys. 119 (2003) 10904–10910.
[20] A.M. Nie, H.S. Yang, Q. Li, X.Y. Fan, F.M. Qiu, X.B. Zhang, Ind. Eng. Chem. Res. 50 (2011) 9944–9948.
[21] X.Y. Fan, F.M. Qiu, H.S. Yang, W. Tian, T.F. Hou, X.B. Zhang, Catal. Commun. 12 (2011) 1298–1302.
[22] W. Tian, H.S. Yang, X.Y. Fan, X.B. Zhang, Catal. Commun. 11 (2010) 1185–1188.
[23] N.Q. Zhao, C. He, J.J. Li, Z.Y. Jiang, Y.D. Li, Mater. Res. Bull. 41 (2006) 2204–2209.
[24] Q. Li, H.S. Yang, A.M. Nie, X.Y. Fan, X.B. Zhang, Catal. Lett. 141 (2011) 1237–1242.
[25] Q. Li, H.S. Yang, X.Y. Fan, F.M. Qiu, X.B. Zhang, J. Hazard. Mater. 192 (2011) 915–921.
[26] F. Bertinchamps, C. Grégoire, E.M. Gaigneaux, Appl. Catal. B 66 (2006) 1–9.
[27] S. Riyas, P.N. Mohan Das, Br. Ceram. Trans. 103 (2004) 23–28.
[28] W.Q. Xu, Y.B. Yu, C.B. Zhang, H. He, Catal. Commun. 9 (2008) 1453–1457.
[29] T. Yamashita, P. Hayes, Appl. Surf. Sci. 254 (2008) 2441–2449.
[30] C.E. Dube, B. Workie, S.P. Kounaves, A. Robbat, M.L. Aksu, G. Davies, J. Electrochem. Soc. 142 (1995) 3357–3365.
[31] S. Poulston, P.M. Parlett, P. Stone, M. Bowker, Surf. Interface Anal. 24 (1996) 811–820.
[32] S. Guerrero, I. Guzmán, G. Aguila, P. Araya, Catal. Commun. 11 (2009) 38–42.
[33] S.A. Halawy, S.S. Al-Shihry, M.A. Mohamed, Catal. Lett. 48 (1997) 247–251.
[34] F.W. Chang, T.C. Ou, L.S. Roselin, W.S. Chen, S.C. Lai, H.M. Wu, J. Mol. Catal. A 313 (2009) 55–64.
[35] H. Sjövall, L. Olsson, E. Fridell, R.J. Blint, Appl. Catal. B 64 (2006) 180–188.
[36] J.M. Fedeyko, B. Chen, H.Y. Chen, Catal. Today 151 (2010) 231–236.
[37] M. Koebel, G. Madia, M. Elsener, Catal. Today 73 (2002) 239–247.
[38] J.A. Sullivan, O. Keane, Appl. Catal. B 70 (2007) 205–214.
[39] Z.G. Huang, Z.P. Zhu, Z.Y. Liu, Q.Y. Liu, J. Catal. 214 (2003) 213–219.
[40] H.H. Phil, M.P. Reddy, P.A. Kumar, L.K. Ju, J.S. Hyo, Appl. Catal. B 78 (2008) 301–308.
[41] Q. Li, H.S. Yang, Z.X. Ma, X.B. Zhang, Catal. Commun. 17 (2012) 8–12.
[42] Z.P. Zhu, H.X. Niu, Z.Y. Liu, S.J. Liu, J. Catal. 195 (2000) 268–278.
[43] G. Delahay, D. Valade, A. Guzmán-Vargas, B. Coq, Appl. Catal. B 55 (2005) 149–155.
[44] H.Y. Chen, T. Voskoboinikov, W.M.H. Sachtler, J. Catal. 186 (1999) 91–99.
[45] B. Frank, G. Emig, A. Renken, Appl. Catal. B 19 (1998) 45–57.
[46] M.A. Vannice, A.B. Walters, X. Zhang, J. Catal. 159 (1996) 119–126.
[47] I. Nova, L. Lietti, E. Tronconi, P. Forzatti, Catal. Today 60 (2000) 73–82.
[48] M.A. Centeno, I. Carrizosa, J.A. Odriozola, Appl. Catal. B 19 (1998) 67–73.
[49] M. Kantcheva, Appl. Catal. B 42 (2003) 89–109.
[50] S. Yamazoe, T. Okumura, Y. Hitomi, T. Shishido, T. Tanaka, J. Phys. Chem. C 111 (2007) 11077–11085.